IEEE Open Journal of
Industry Applications

Received 21 September 2020; revised 18 December 2020 and 9 February 2021; accepted 23 February 2021. Date of publication 3 March 2021; date of current version 24 March 2021. The review of this article was arranged by Editor H. W. Kim.

Digital Object Identifier 10.1109/OJIA.2021.3063625

Universal Active Power Control Converter for DC-Microgrids With Common Energy Storage

UMAMAHESWARARAO VUYYURU [1] (Student Member, IEEE), SUMAN MAITI [2] (Member, IEEE), CHANDAN CHAKRABORTY [2] (Fellow, IEEE), AND EFSTRATIOS I. BATZELIS [3] (Senior Member, IEEE)

[1] School of Energy Science and Engineering, Indian Institute of Technology Kharagpur, Kharagpur, West Bengal 721302, India
[2] Department of Electrical Engineering, Indian Institute of Technology Kharagpur, Kharagpur, West Bengal 721302, India
[3] School of Electronics and Computer Science, University of Southampton, Southampton SO17 1BJ, U.K.

CORRESPONDING AUTHOR: UMAMAHESWARARAO VUYYURU (e-mail: umamahesh271@gmail.com)

This work was supported in part by the Department of Science and Technology (DST), India, under the Project U.K. India Clean Energy Research Institute (UKICERI) under Grant DST/RCUK/JVCCE/2015/02 (C) and in part by the Royal Academy of Engineering under the Engineering for Development Research Fellowship Scheme under Grant RF/201819/18/86.

ABSTRACT This paper presents a battery integrated Power Flow Controller (PFC) which is found effective for the interconnection of several dc microgrids. The configuration offers delicate control over load-flow and also provides a way for the integration of Common Energy Storage (CES) to the adjacent grids. The CES is more effective when both the grids have surplus or deficit of power compared to their individual storage capacity (if any). In this paper, a Universal Active Power Control Converter (UAPCC) is proposed (which is basically a three-port converter), where port-1 is connected in parallel with the line, port-2 is connected in series with the line, and port-3 is connected to the CES through a bidirectional dc-dc converter. Relevant control algorithms have been developed for the operation of such system satisfying various system requirements that are inevitable for the interconnection of dc microgrids. The proposed control methods allow decoupled operation of three ports to control power flow between dc grids and CES independently. The complete system along with control methods are initially verified through computer simulation using MATLAB/SIMULINK. Thereafter, a prototype is developed in the laboratory at 380 V level to experimentally validate the concept. The results show effectiveness of the UAPCC for interconnection of dc microgrids with CES.

INDEX TERMS Common Energy Storage (CES), DC microgrids, DC power flow controller, DC-DC converters, renewable energy sources (RES).

I. INTRODUCTION

The microgrid is an independent system that usually comprises of renewable sources, energy storage systems and different kinds of loads [1], [2]. This is an attractive solution to electrify the remotely located rural areas, building automation, etc. [3]. DC microgrids carry more advantages in contrast with the ac counterpart especially in terms of efficiency, flexibility, density of power, absence of reactive power and frequency etc., [4]–[6]. Moreover, dc microgrids can be considered as an optimized scheme for low-voltage residential, more electric aircraft, advanced automotive systems and commercial applications [7]–[9]. Isolated microgrids may derive its sources of energy mostly from PV and wind. However, weather conditions affect the output power of PV and wind generation systems. In such systems, Battery Energy Storage System (BESS) plays an important role in taking care of the surplus and/or deficit power that will help in maintaining the dc bus voltage by charging and discharging the battery accordingly [10], [11]. In situations of surplus power goes beyond the charging capacity of battery, the only option to control the dc bus voltage is to deviate from MPP operation. As a result, there will be a reduction in the utilization of renewable energy sources. Conversely, in case of deficit power, load shutdown should happen to regulate the dc bus voltage. Running of unplanned appliances such as welding and drilling machines may demand additional power from the individual microgrids. Therefore, an additional storage is required for balancing the demand and generation, which can increase system reliability

[12]. Moreover, oversizing of capacity of renewable energy sources (RES) and BESS may increase cost of investment and can result in underutilization of RES [13].

RES can be utilized properly with the use of interconnection of dc microgrids. This may assist in reducing the investment cost by sharing of surplus or deficit power between microgrids [14]–[16]. Needless to say that power transfer in a dc network is dependent only on network resistance and potential difference between both ends of the network. A distributed control system is implemented in [17] to regulate the power flow between interconnected dc microgrids by adjusting the voltage set points of individual microgrids. Coupled control algorithms affect the control of power transfer, flexibility, plug-and-play feature of dc microgrids and therefore results in reducing of scalability of microgrid-cluster [18]. Moreover, adjustment of bus voltages cannot ensure power flow on each interconnected link in a multiple bus network. It is important to mention that power flow cannot happen between buses when both the buses maintain equal potential. Thus there is a need for a power electronics based power flow controller (PFC) to allow and regulate the power flow in such cases [19].

A non-isolated cascaded bi-directional buck-boost based converter is presented in [20], which deals with the control of power flow between microgrids. A power flow converter based on dual active bridge topology is proposed in [21], [22], that maintains the input and output voltages in limits, thereby controlling the power transfer. In these topologies, the PFC is connected in shunt and its input and output voltages are rated more or less equal to the grid voltage magnitudes. Therefore, the rating of PFC has to be same with the power that needs to be transferred between the grids. To reduce the rating of the shunt connected PFCs, series connected converters are proposed [23], such as Controlled Series Current Compensator (CSCC) [24], Floating Bidirectional Power Flow Controller (F-BPFC) [25], and Load Flow Converter (LFC) [26]. Basically these series connected converters create a potential difference between two buses by injecting controlled voltage in series with the line. The series voltage injection generates a positive resistance effect which increases the dc line current, or alternatively, a negative resistance for decreasing line current. Therefore, required amount of power flow can take place.

In the process of controlling surplus or deficit power between the interconnected microgrids, there will be transmission loss due to line resistance. These losses are considerable, particularly when the distance between the grids are comparatively high (in the range of 500 m to 2 km) and the voltage level is low [27], [28]. Moreover, PFC alone may not work, when there will be surplus or deficit power (at the same time) on both grids of an interconnected dc microgrid system in comparison of their BESS capacity. In such cases, a common energy storage (CES) might be of use that can help in balancing the demand and generation of power between the grids without having to increase the power capacity of the existing microgrids [29]. Furthermore, CES can increase the rate of energy access and decrease the line loss by supporting additional active power.

TABLE 1. Comparison of UAPCC With Other Existing PFCs

List of PFCs	Bi-directional power flow	External power supply	Rating of the converter	Concept of CES integration
Bi-directional buck-boost [20]	Possible	Not required	Same as power rating that needs to be transferred	Not explored
Dual active bridge [21], [22]	Possible	Not required	Same as power rating that needs to be transferred	Not explored
Controlled series current compensator (CSCC) [24]	Not possible	Required	Less compared to power that needs to be transferred	Not explored
Floating bidirectional power flow controller (F-BPFC) [25]	Possible	Required	Less compared to power that needs to be transferred	Not explored
Proposed converter (UAPCC)	Possible	Not required	Less compared to power that needs to be transferred between grids	Investigated in this manuscript

In this paper, the Universal Active Power Control Converter (UAPCC) is proposed for power-flow control between microgrids with CES, which increase the power access and control capability. Basically, UAPCC has three ports. Port-1 (i.e. input of DAB) is connected parallel to the dc line whereas port-2 is output of full-bridge dc-dc converter which is connected in series with the dc line. Port-3 has bidirectional dc-dc converter facilitating power transfer with the CES. Table 1 shows the comparison of proposed converter with the existing PFCs in the literature. The UAPCC works as a self-exited system with multi-directional power flow capability. A dynamic voltage with appropriate magnitude and polarity will be injected in series with the distribution line with the help of UAPCC. This makes power flow control in multi-directional among grid-1, grid-2 (of interconnected microgrids) and the CES. The main contributions of this paper are as follows.

- A new three port converter is proposed for power flow control and integration with CES.
- A Decoupled control method is proposed to allow independent operation of three ports in UAPCC to manage power flow between grids and CES.
- A reference power selection logic is derived with the support from CES to reduce line loss in the system.
- Analysis of power flow control between interconnected microgrids with and without CES is studied.
- A method to estimate the size of CES is also presented by considering uncertainties in an interconnected microgrid system.
- Finally, the configuration and the proposed control methods are validated through simulation and then experimentally verified through a laboratory developed hardware prototype.

This paper is organized as follows; Section I has put forward the need of common energy storage system for interconnection of dc-microgrids and its associated literature. Interconnection of microgrids through PFC with and without CES are discussed in Section II. Section III explains the proposed

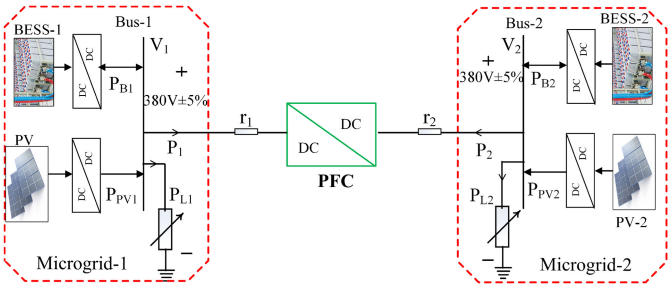

FIGURE 1. Interconnection of dc microgrids through PFC.

topology and working principle. Section IV elaborates the overall control strategy of the system and sizing of CES is explained in Section V. Simulation and experimental verification of various operating modes are covered in Section VI and Section VII, respectively. Section VIII presents the conclusions.

II. INTERCONNECTION OF DC MICROGRIDS THROUGH PFC WITHOUT COMMON ENERGY STORAGE (CES)

This section explains the need of CES support for the interconnected microgrids. Fig. 1, shows the interconnection of two dc microgrids though PFC without CES. Here the two microgrids are formed by PV, BESS and internal loads, where P_j is the net power at j-th bus ($j \in 1, 2$), $P_{PV\,j}$, P_{Bj}, P_{Lj} are the power associated to PV, battery, and load for j-bus ($j \in 1, 2$), respectively. The advantage of PFC is already explained in Section I and there are sufficient literature available [19]–[26] for power flow control using PFC. Some issues related to PFC alone for interconnected dc microgrid system are listed in the following section.

- It is observed in an interconnected dc grids that power may back-and-forth in between two microgrids due to fluctuation of load and generation profile, as depicted in Fig. 2 (a). Because of this, the loss in an interconnected system increases as reported in [30]. It is also well investigated that a fluctuating type power profile of transmitted power causes more loss than a constant type power profile [31].
- PFC alone may not work, if both the grids are having either surplus or deficit of power compared to their BESS capacity. In that scenario, load scheduling or generation curtailment is required to manage the interconnected system.

To address the aforesaid limitations, a Common Energy Storage (CES) is attached to PFC as shown in the Fig. 2 (b). The combination of PFC and CES has many advantages which are highlighted in the following section.

- The proposed concept of CES with PFC can reduce the variation of net power by coordinating dc-grids and CES which reduces losses of the overall system. The local BESS takes care most of the power fluctuation within the dc microgrid and the remaining power (surplus or deficit) which is almost constant is transfered via tie-line to CES or other microgrid. Therefore, a smooth active power exchange is possible between microgrids with the help of CES.
- Transmission loss can be reduced drastically under the presence of CES which is explained with an example in Section III.
- The CES can absorb or deliver power (surplus or deficit) to both the grids at the same time.

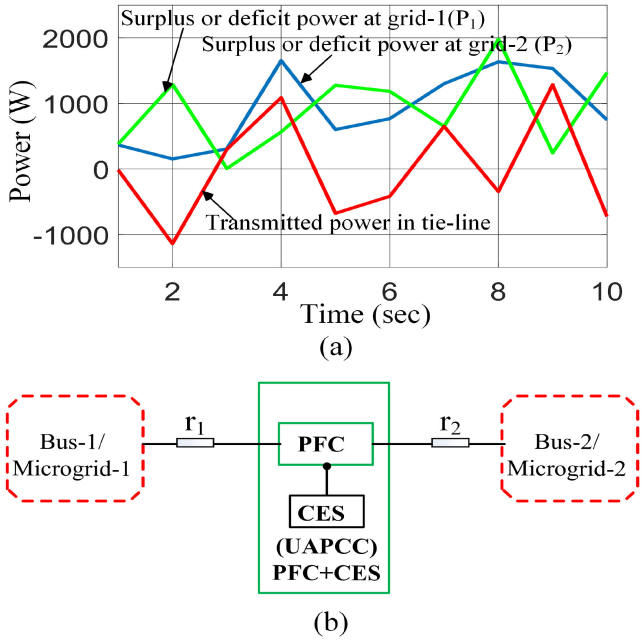

FIGURE 2. (a) Sharing power between microgrids with PFC (b) Proposed configuration, i.e. CES integrated with PFC.

III. CONFIGURATION AND WORKING PRINCIPLE OF UAPCC (PFC+CES)

A. CONFIGURATION OF UAPCC

The proposed configuration of three-port UAPCC is shown in Fig. 3. The operation of the converter is explained briefly as follows.

The port-1 and port-2 are connected to the dc line, one in parallel and the other in series. Therefore, isolation is required between these ports. High voltage conversion ratio is also needed because the voltage at port-1 (V_3) of UAPCC is nearly equal to grid voltage, whereas voltage at port-2 (V_s) will be less compared to grid voltage. Based on parameters considered in this work, the series voltage (V_s) will be topically less than 20% of the grid voltage. Note that V_s mainly depends on the line parameters, grid voltages, and amount of power to be transferred between the grids. Moreover, bidirectional power flow support is required at port-1 to exchange power with port-2 and port-3. Considering all of these requirements, an isolated high gain bi-directional dc-dc converter is the best suitable choice to form port-1 and port-2 of UAPCC. A dual active bridge converter is chosen for this application as it can provide isolation between input and output, high efficiency, and has moderate power rating [32]–[34]. Input of DAB forms port-1 which is connected in parallel to the dc line,

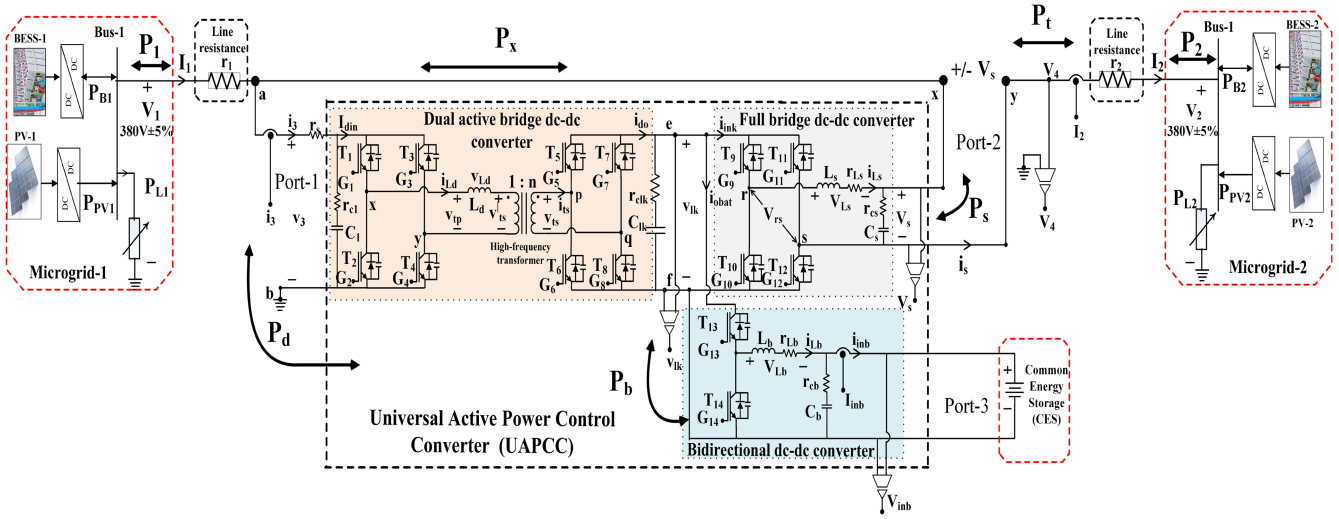

FIGURE 3. The interconnection of dc microgrids with UAPCC.

and the output of DAB forms an intermediate dc-link from which port-2 and por-3 are derived using dc-dc converters. Here, DAB maintains a fixed dc-link voltage (V_{lk}) which can be achieved by adjusting phase-difference between V_{tp} and V_{ts} [35].

Port-2 is connected in series with the dc tie-line. A full-bridge dc-dc converter [36] is employed just after intermediate dc bus to adjust the voltage of port-2. The main objective of port-2 is to control power flow between two dc-grids by injecting desired potential in series with the tie-line. The series injected voltage, i.e. V_s can be either positive or negative depending on the direction of power flow. The power flow is taken place from bus-2 to bus-1 when the injected series voltage is positive, whereas the reverse phenomena is happened if the voltage is negative.

The Port-3 of UAPCC is formed by dc-dc bi-directional converter [37] which exchanges power with CES. Therefore, this converter is being referred to as CES-converter whose input is fed from the DAB. Note that the voltage of intermediate bus (i.e. V_{lk}) is higher than the voltage of port-3. Switches T_{13} and T_{14} operate in complementary fashion, based on duty ratio. The charging and discharging operation of CES can be regulated according to the power requirements at grid-1 and grid-2 as shown in Fig. 3. Charging of the CES is happened via DAB, when one of the two grids (or both) have surplus of power. Similarly, discharging of CES is taken place through port-1 of DAB when power needs to be transfered to support the grids.

From Fig. 3 and the above discussion, it can be noted that the power rating of CES-converter depends on the capacity of CES. Although the full bridge converter is carrying line current, the power rating of this converter is significantly less because of its output voltage requirement being very low compared to the dc bus voltages. As DAB converter has to support power flow to both full-bridge and CES-converters, its rating will be equal to sum of the power ratings of the two.

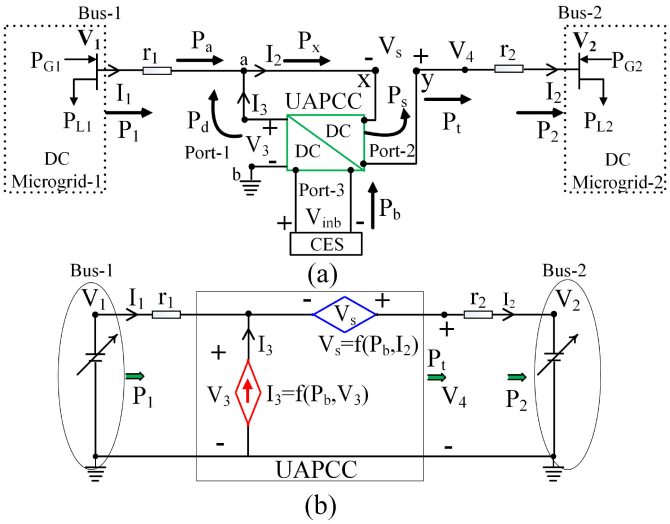

FIGURE 4. (a) Connection diagram of UAPCC (considering power flow from grid-1 and CES to grid-2) (b) Equivalent circuit of system under consideration.

B. WORKING PRINCIPLE OF UAPCC

The complete system of Fig. 3 can be represented in the form of block diagram which is illustrated in Fig. 4 (a). Here P_{G1}, P_{L1}, P_{G2} and P_{L2} represent the total generation and load powers at bus-1 and bus-2, respectively. Note that the total generated power includes a local energy storage at both the grids. Power flow associated to CES is represented by P_b which can be positive or negative depending on the operation of CES-converter. P_d and P_s are the powers at port-1 and port-2 of UAPCC, respectively.

Power flow between grid-1 and grid-2 including CES can be analyzed by deriving suitable expression for P_t. This can be done in different ways, viz. power from grid-1 to grid-2, grid-2 to grid-1, with and without CES, etc. One of such modes of power flow (from both grid-1 and CES to grid-2) is considered

here to derive an expression for P_t. During this mode of operation, Fig. 4 (a) can be represented by an equivalent circuit as given in Fig. 4 (b) and the corresponding explanation is as fallows.

- Microgrids involving bus-1 and bus-2: The coordinated control among PV and BESS takes the responsibility to regulate dc bus voltage. Here the combination of all sources at one node is modelled as a voltage source (V_1 and V_2).
- Distribution line: The distribution line is modelled using two lumped resisters (r_1 and r_2).
- Proposed three-port converter (i.e., UAPCC): The UAPCC is modelled by neglecting losses in the converter. It is assumed that power is flowing towards bus-2. To make this happen, the potential at node-y should be greater than the potential of bus-2. Using port-2 of UAPCC, the required controlled voltage (V_s) can be injected in series with the line to make the node-y voltage more than the bus-2 voltage. The series injected voltage is dependent on the amount of power transferred in the line and the power from the CES. Therefore, port-2 can be modeled as a controlled voltage source as a function of line current (I_2) and CES power (P_b). In this mode of operation, power from CES flows from port-3 to port-1 via bidirectional dc-dc converter and DAB. The current at port-1 mainly depends on the voltage at port-1 and power from CES (i.e., from port-3). Therefore, the port-1 and port-3 of UAPCC can be modeled as a controlled current source (I_3). The current I_3 is a function of port-1 voltage (V_3) and CES power (P_b).

Here V_1, V_2 are voltages of bus-1 and bus-2, r_1, r_2 indicate line resistances of distribution line, V_3 and I_3 are input voltage and current of port-1. Voltage and current of port-2 are given by V_s and I_s. V_4 is the voltage at node just after UAPCC and I_1, I_2 are the net currents related to grid-1 and grid-2. P_1 is the net-power coming out from grid-1, and P_2 is the net-power entered into grid-2. Power at node V_4 can be expressed as

$$P_t = V_4 I_2 \tag{1}$$

According to Fig. 4 (b),

$$I_2 = \frac{V_4 - V_2}{r_2} = I_1 + I_3 = \frac{V_1 - V_3}{r_1} + \frac{P_b}{V_3} \tag{2}$$

$$V_4 = V_2 + I_2 r_2 \tag{3}$$

$$V_3 = V_4 - V_s \tag{4}$$

Using (1), (2), (3) and (4), P_t can be written as:

$$P_t = \frac{r_2}{r_1^2}(V_1 - V_3)^2 + \frac{P_b r_2}{V_3}\left(\frac{P_b}{V_3} + \frac{2V_1}{r_1} + \frac{V_2}{r_2}\right) + \frac{1}{r_1}(V_2 V_1 - 2P_b r_2 - V_2 V_3) \tag{5}$$

Expression of P_t for any other mode of operation can be obtained from (5) by incorporating sign of the conventions appropriately.

C. MODES OF OPERATION

The operation of UAPCC can be described through different modes of operation as graphically illustrated in Fig. 5. Here the power flow directions between grids and CES though UAPCC are represented with the assumptions of zero losses in converter (UAPCC) and transmission line. Fig. 5 (a) shows mode-1 operation of UAPCC, where power flow is taken place from grid-1 and CES to grid-2. This situation may occur when deficit of power at grid-2 is more than the available excess power at grid-1. In this condition, to meet the load demand at grid-2, an additional power is required which comes from grid-1 and CES through UAPCC as shown in Fig. 5 (a). In the similar way, rest of the operating modes can be explained.

D. AN EXAMPLE TO EXPLAIN THE WORKING PHILOSOPHY OF UAPCC

An example is considered here to further explain the working philosophy of UAPCC. Let us assume that a power of 0.5 kW is considered to be transferred between grids where the dc bus voltages of grid-1 and grid-2 are fixed at 380 V with a variation of (±5%) owing to uncertainty in renewable generation. P_t and P_b are assumed to be varied from -0.5 kW to 0.5 kW. Using (5), the required series voltage is computed through MATLAB program and the same is plotted in Fig. 6 for different grid voltages. The point C_1 indicates that the maximum amount of power (e.g. 0.5 kW) is flowing from grid-1 to grid-2 with CES is in charging mode at its maximum capacity (e.g. -0.5 kW), and grid voltages are kept at different voltage levels (e.g., $V_1 = 360\,V$ & $V_2 = 400\,V$). In this situation, a total power of 1 kW (0.5 kW to grid-2 + 0.5 kW to CES) is drawn from grid-1 by applying a voltage of 59.2 V in series with the line (i.e. $V_s = 59.2\,V$). Similarly, at point C_2, just opposite situation is occurred, where $V_s = -59.9\,V$ is required to make the power flow happen. Therefore, it can be concluded that the magnitude of series voltage is quite low (here it is 16%) compared to the grid voltage. Using this data, in this work, the output voltage of DAB (V_{lk}) is set at 60 V to meet the requirements.

Fig. 7 shows the line losses (P_{loss}) vs. transmitted power (P_t) with and without CES support. Note that + P_t indicates power flow into the grid-2, and - P_t represents power flow in the opposite direction. Here the line losses are plotted for a range of P_t (+600 W to -600 W) considering different level of support from CES. The support from CES is gradually increased up to 500 W with a step of 100 W which are indicated by P_{b1} to P_{b5} in the figure. It is observed that the line losses are reduced for a particular P_t when power support from CES is gradually increased. The study can be easily extended to investigate the reverse power flow (i.e., CES to grid-1). From the figure, it is observed that the magnitude of line loss depends on the power flow through the line. Power loss in the line is nearly 26 W ($I_1^2 r_1 + I_2^2 r_2$) when $P_b = 0$ W (i.e., without CES support), and the line loss decreases with the support from CES. It clearly indicates that the line loss is reduced by almost 50% (13 W) with the maximum support

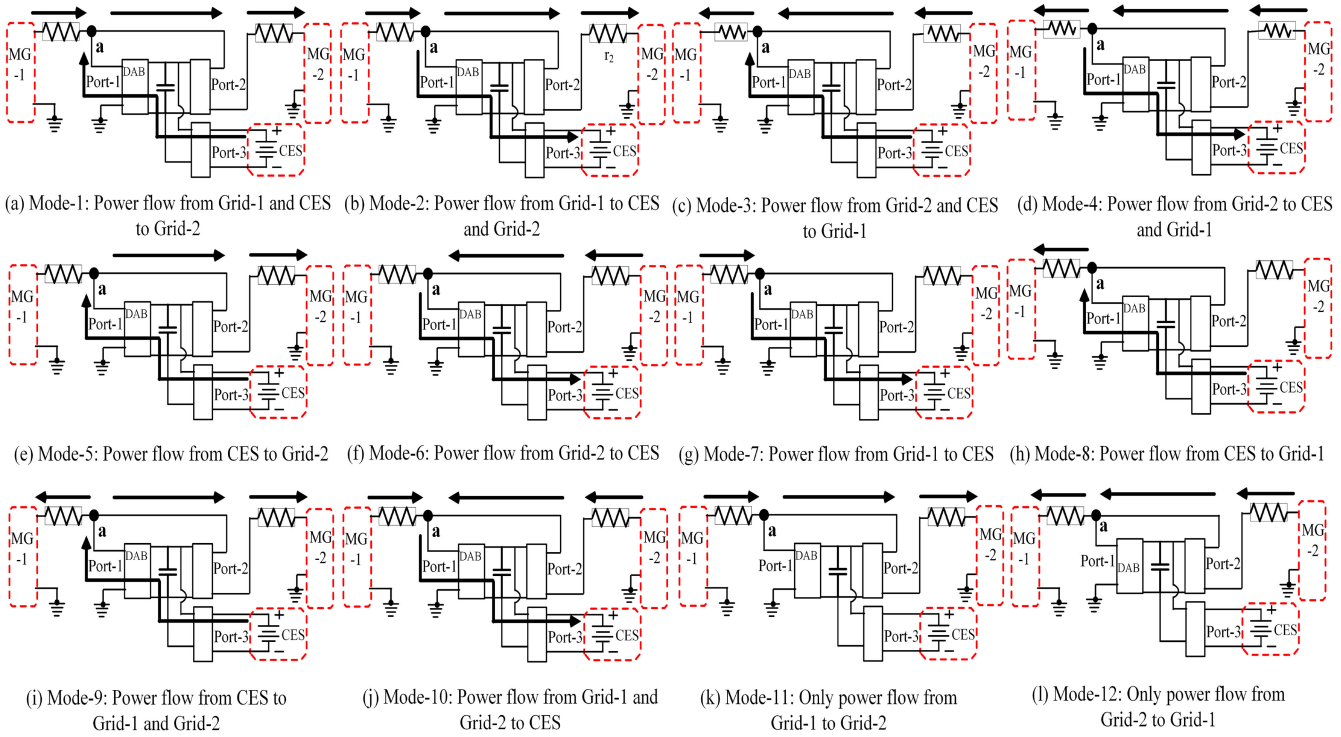

FIGURE 5. Pictorial representation of modes of operation of UAPCC.

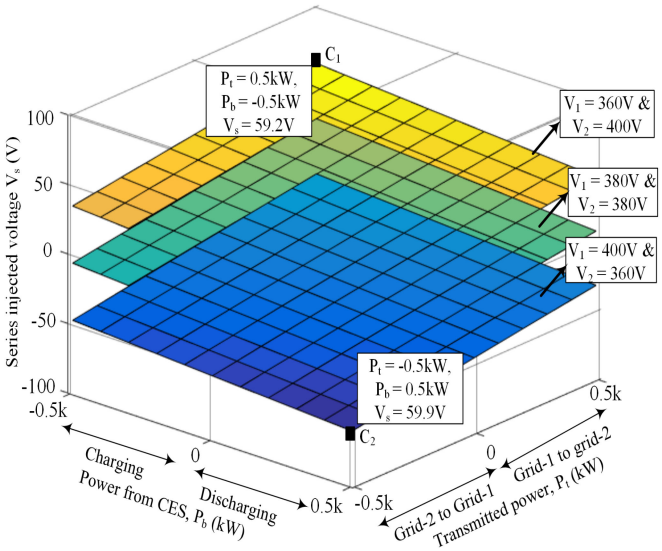

FIGURE 6. Power (P_t, P_b) vs. series voltage (V_s) for different grid voltage levels: $r_1 = 5\Omega$ and $r_2 = 5\Omega$.

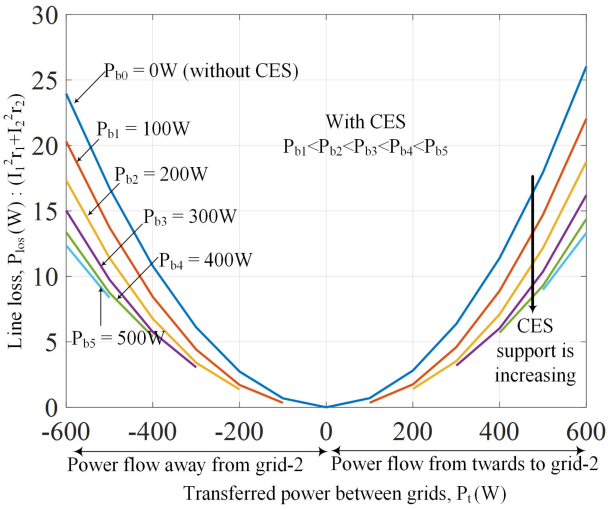

FIGURE 7. Line losses with and without CES support ($r_1 = 5\Omega$, $r_2 = 5\Omega$, and $V_1 = V_2 = 380\,V$).

from CES (i.e., 500 W). The CES is more effective when the microgrids are far from each other, and they are connected through a long tie-line.

IV. SYSTEM CONTROL

A. CONTROL OF UAPCC

The proposed control block diagram of UAPCC is shown in Fig. 8, together with feedback variables and control signals. Control of the converter connected to each port of UAPCC is important to regulate the active power flow between dc grids and CES. The proposed control strategy allows each converter to operate independently, which enables the simple power flow control. Here P_1 and P_2 are the net-powers available at microgrid-1 and microgrid-2, respectively which are generated by local power control strategies of individual dc microgrids. In this work, P_1, P_2 are considered to be known and are fed as inputs to Reference Power Selection Logic (RPSL) of UAPCC. Flowchart for the operation of RPSL is shown in Fig. 9 which mainly depends on the SoC of CES

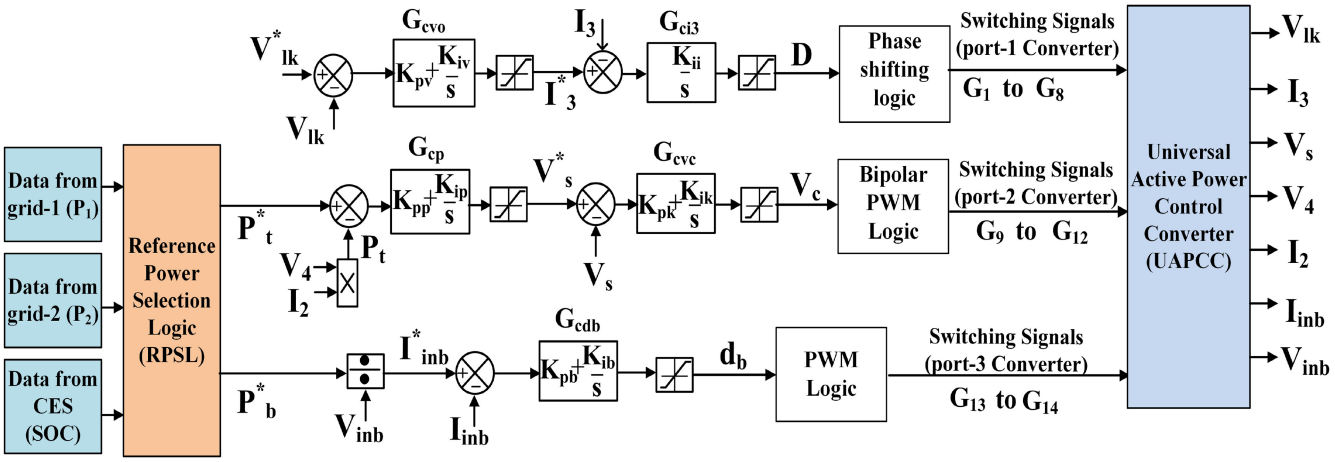

FIGURE 8. The overall control of UAPCC.

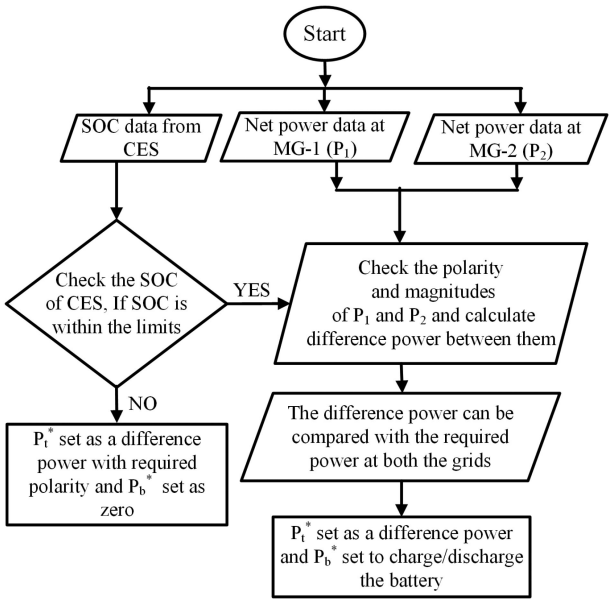

FIGURE 9. Flowchart for Reference Power Selection Logic (RPSL).

and the available net power (P_1 and P_2) at both the grids. Using these values, RPSL generates P_b^* and P_t^*. Note that the optimal electricity trading between the grids and CES is not discussed in this work to reduce the line loss. This work is mainly focused on the control of power flow between grids and CES using UAPCC. There are various operating modes exist to check the performance of UAPCC. The control of UAPCC is elaborated here for one of the modes and the operation for other modes can be explained in the similar way.

B. POWER FLOW FROM DC GRID-1 TO CES AND DC GRID-2

In this mode of operation, the available excess power at grid-1 is more than the deficit power at grid-2 and SoC of CES is within the limits. The power flow in the distribution line towards grid-2 is controlled by port-2 converter and the power flow from grid-1 to CES or vice-versa is controlled by port-1 and port-3 converters of UAPCC.

Port-1 converter (i.e., DAB), consists of two control loops, which are outer voltage-loop and inner current-loop. Regulation of output voltage of DAB by controlling the power flow on port-1 and port-3 is the primary goal of this control.

The input PI controller processes the error signal which is the difference between reference and actual values of V_{lk} ($e = V_{lk}^* - V_{lk}$). Accordingly a reference current (I_3^*) is generated for the inner current loop. Current controller (G_{ci3}) receives the current-error signal and generates phase-shift, D required for the DAB. D varies from -0.5 to 0.5. Thus, the power flow takes place from input (V_3) to output (V_{lk}) of DAB or vice-versa [38].

The reference power commands (P_b^* and P_t^*) for the port-2 and port-3 converters of UAPCC are received from RPSL (as shown in Fig. 9) based on requirements of individual dc-microgrids. The negative series voltage (with respect to output voltage of port-2) is required to create the higher potential at point 'y' (i.e., V_4) compared to grid-2 voltage (V_2). Thus, the required power flows to grid-2 based on the magnitude of V_s. Similarly, in reverse power flow case, the required series voltage is positive to create lower potential at point 'y' compared to grid-2 voltage (V_2). The power controller (G_{cp}) and voltage controller (G_{cvc}) together generates switching signals to the devices T9 to T12 to control the output voltage (V_s) of full-bridge converter [26]. This is mentioned in Fig. 8. It is to be noted that, the power P_t^* can take both positive and negative values depending on power flow direction. If P_t^* is positive, power flow will be towards grid-2. Similarly, negative polarity indicates the reverse power flow.

CES can be charged or discharged based on the power-flow command generated from RPSL. CES should charge only when the loads are low, in other wards, when there is an excess generation available at single or both the grids of an interconnected dc microgrid system. CES should discharge when source cannot or can only marginally meet the load demands, in other words sources have no excess generation

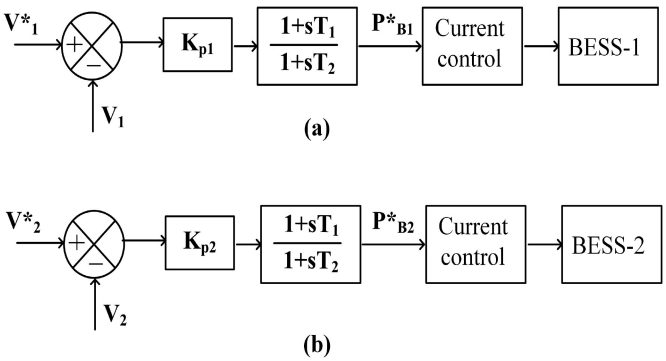

FIGURE 10. BESS control: (a) Microgrid-1 and (b) Microgrid-2.

capacities at single or both the grids of an interconnected dc microgrid system. Power data available at grid-1, grid-2 and CES is used to generate the power-command P_b^* using RPSL. which further generates the current reference I_{inb}^* for the battery-converter according to (6).

$$I_{inb}^* = \frac{P_b^*}{V_{inb}} \tag{6}$$

With this current reference, error in current is processed to generate the gating pulses for the switches T13 and T14.

C. CONTROL OF MICROGRIDS

As assumed BESS at both the microgirds are sufficient. The transmitted power in the line (P_1 or P_2) will be constant and acts as constant power source. Thus, the BESS-1 and BESS-2 are controlled to maintain the dc voltage of microgrid-1 and microgrid-2 respectively. The control logic of the BESS is identical for both the microgrids and is shown in Fig. 10. Here a voltage droop control scheme [39] is used to regulate the dc bus voltage. K_{p1} and K_{p2} are droop coefficients determines the dc voltage variation during power changes in the microgrids. Larger K_{p1} and K_{p2} are preferred for smaller deviations in dc bus voltage. A lead-lag filter is serialized with the voltage droop controller to filter out high frequency noises and enhance system damping. To balance the power flow in a microgrids, the required power from the BESS are:

$$P_{B1}^* = P_1 - P_{PV1} + P_{L2} \tag{7}$$

$$P_{B2}^* = P_2 - P_{PV2} + P_{L2} \tag{8}$$

Power references P_{B1}^* and P_{B2}^* further generates the current references for the battery converters for current controllers.

V. SIZING OF CES

Intermittent outputs of distributed generation systems like PV (at grid-1) and wind (at grid-2) are considered for the sizing of CES system (see in Fig. 3). Here, sizing of CES is decided based on the net-powers (P_1 and P_2 available at both the microgrids. Expressions of P_1 and P_2 are as follows.

$$P_1 = P_{G1} - P_{L1} \tag{9}$$

$$P_2 = P_{G2} - P_{L2} \tag{10}$$

where P_{G1}, P_{L1}, P_{G2} and P_{L2} represent the total generation and load powers at dc-grid-1 (bus-1) and dc-grid-2 (bus-2) respectively. Note that local energy storage is employed in both the microgrids to support only critical loads. For the ease of analysis, the local energy storage is included within the generation power for both the stations. Here P_1 and P_2 are highly dependent on the uncertainty of generations and loads of microgrid-1 and microgid-2 respectively. In stochastic optimization methods, forecasted wind, PV, and load powers are used to find the optimal sizing of the system [40]. In this work, the Robust Optimization (RO) technique is used for finding the size of CES [41]. RO only requires limited information of the uncertainty set such as the mean, lower and upper bounds of the uncertain data which are easier to obtain from forecasted or estimated with certain confidence intervals in practice [42]. In this paper, the uncertainty sets of PV and wind energy generation as well as load consumptions at Microgrid-1 and 2 are introduced under the given uncertainty limits [43]. The uncertainty set for load consumption at microgrid-i (P_{Li}) at each time interval t in a day d can be expressed as

$$W_{d,t}^{Load} = \left\{ w_{i,d,t}^{Load} \right\},\ w_{i,d,t}^{Load} \epsilon \left[\underline{w}_{i,d,t}^{Load}, \overline{w}_{i,d,t}^{Load} \right] \tag{11}$$

Here, the load power consumption at microgrid-i at time t (i.e., hour index) in a day d is described by the interval $[\underline{w}_{i,d,t}^{Load}, \overline{w}_{i,d,t}^{Load}]$, where $W_{d,t}^{Load}$ is uncertainty set of load power, $w_{i,d,t}^{Load}$ is uncertainty load power data at time t, and $\underline{w}_{i,d,t}^{Load}, \overline{w}_{i,d,t}^{Load}$ are lower and upper bounds of $w_{i,d,t}^{Load}$. Similarly, the uncertainty sets for PV and wind generations (considering 5 kW maximum) at each time interval t in a day d are expressed as

$$W_{d,t}^{PV} = \left\{ w_{i,d,t}^{PV} \right\},\ w_{i,d,t}^{PV} \epsilon \left[\underline{w}_{i,d,t}^{PV}, \overline{w}_{i,d,t}^{PV} \right] \tag{12}$$

$$W_{d,t}^{Wind} = \left\{ w_{i,d,t}^{Wind} \right\},\ w_{i,d,t}^{Wind} \epsilon \left[\underline{w}_{i,d,t}^{Wind}, \overline{w}_{i,d,t}^{Wind} \right] \tag{13}$$

When the generation power (including the discharging capacity of each local energy storage) at microgrid-1 and 2 is not enough to meet the load demand, the CES needs to be discharged to balance the power demand, which can avoid the critical load shut-down at the grids. Minimum energy supplied by the CES in a day for one set of uncertainty is defined as

$$C_{dis}^{min} = \int_0^T \left(w_{1,d,t}^{P1} + w_{2,d,t}^{P2} + P_{loss} \right) \delta t \tag{14}$$

where T is total number of hours in a day; δt is the time interval of one hour in this paper; $w_{1,d,t}^{P1} = w_{1,d,t}^{Load} - w_{1,d,t}^{PV}$ and $w_{2,d,t}^{P2} = w_{2,d,t}^{Load} - w_{2,d,t}^{Wind}$ are the net-powers at time t in microgrid-1 and 2 respectively. P_{loss} is the total losses in the UAPCC and distribution line, which are assumed 5% of power transfered.

When the generation power (including the charging capacity of each local energy storage) at microgrid-1 and 2 is more than the load demand, the CES needs to be charged to increase the utilization of RES. In this case, the minimum energy charged to CES in a day for one set of uncertainty can

TABLE 2. Constraints for the Sizing of CES

Constraints	Expression
Real power balance	$P_{CES}(t) = P_1(t) + P_2(t) + P_{loss}(t)$
Charging and discharging limits	Discharge: $C(t+1) = C(t) - \delta t P_t^d / \eta_{dis}$ Charge: $C(t+1) = C(t) + \delta t P_t^d \eta_{cha}$
Power limits	$0 \le P_t^d \le P^{d,max}$ $0 \le P_t^c \le P^{c,max}$
Stored capacity limits	$C_{min} \le C(t) \le C_{max}$
Starting and ending capacity	C(0) = C(T)

be defined as

$$C_{cha}^{min} = \int_0^T \left(w_{1,d,t}^{P1} + w_{2,d,t}^{P2} - P_{loss} \right) \delta t \tag{15}$$

At the end of the day, minimum required value of CES rating for one set of random generated values for a day can be obtained as [44]

$$C_{CES}^{min} = \max \left(\frac{C_{dis}^{min}}{\eta_{dis}}, \eta_{cha} C_{cha}^{min} \right) \tag{16}$$

where η_{dis} and η_{cha} are the discharging and charging efficiencies respectively, which are take as 0.95 each.

The max-min robust optimization problem for the size selection of CES is described below, where the objective function can be expressed in (17).

$$\underset{C \epsilon X}{MAX} \{C_W^{min}\} \tag{17}$$

The above objective function should satisfy all the constraints given in Table 2, where X is the feasible set of CES size (C) for all constraints; C_W^{min} is the minimum capacity of the CES for uncertainty sets of W; P_t^d and P_t^c are the powers discharged and charged by the CES during time period t; $C(t)$ is the energy stored in the CES at time t; $P^{d,max}$ and $P^{c,max}$ are the maximum discharging and charging powers; C_{max} and C_{min} are the maximum and minimum energy stored in the CES; $C(0)$ is the initial stored energy; and $C(T)$ is the energy balance of CES at the end of the day.

A flowchart of the max-min RO algorithm is shown in Fig. 11. This algorithm gives the solution for worst-case performance of the uncertainty sets of input data. Fig. 12 shows the set of feasible energy storage values for all iterations. Here the maximum value (i.e., 70 kWh) is selected based on max-min RO algorithm at 618^{th} iteration (which is the worst scenario out of 10000 iterations). The corresponding generation and load profiles at microgrid-1 and 2 are shown in Fig. 13. For the same iteration, charge and discharge powers in every hour in a day along with the SoC of CES are shown in Fig. 14. It clearly indicates that the selected capacity of the battery is sufficient to satisfy all the constraints.

VI. SIMULATION RESULTS

This section presents the performance of the UAPCC through simulation. The proposed system as shown in Fig. 3 is modeled and simulated using MATLAB-SIMULINK at 380 V level. The simulation parameters corresponding to Fig. 3 are given in Table 3. Fig. 15 shows the simulation results for dynamic power flow control between grids and CES using

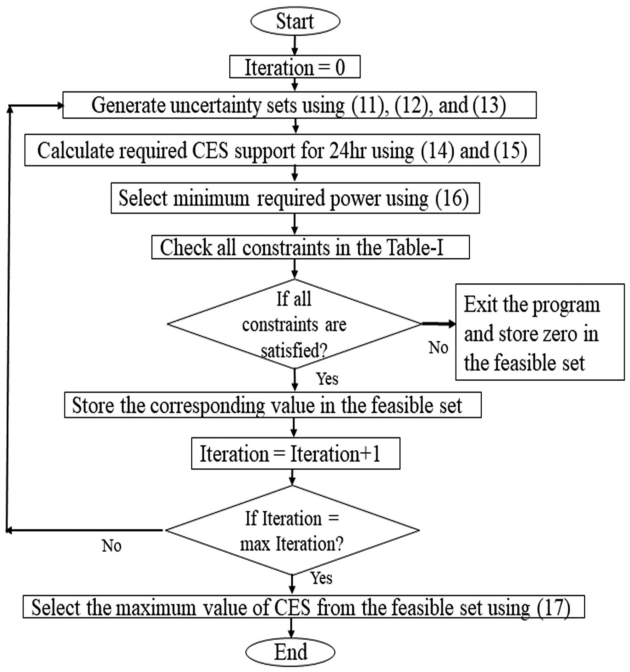

FIGURE 11. Flowchart of the max-min robust optimization algorithm.

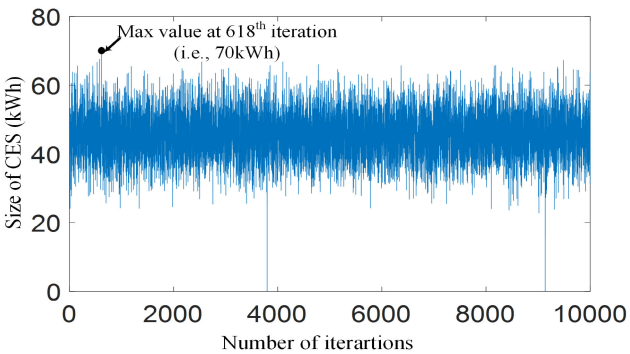

FIGURE 12. Values of energy storage for different iterations.

UAPCC. Here three modes are considered (all possible modes are given in experimental results) to check the dynamic response of the system.

A. POWER FLOW FROM BOTH THE GRIDS TO CES

This situation may occur when the net power generation (including the charging capacity of each local energy storage) is more than the load demand at both the grids. Corresponding results are shown in Fig. 15 (from 1 sec to 3 sec), where an excess power (P_b) of 200 W is being taken from both the grids (100 W from each grid) to charge the CES based on the reference command generated by RPSL. A small series voltage (V_s), around 0.02 V is enough to transfer 100 W (P_t) from grid-2 to port-1. The remaining 100 W is coming from grid-1, which can be represented in terms of current I_1. The magnitude of I_1 is more than I_2 because the extra power is taken from the grid-1 for operation of UAPCC. An illustration of power flow directions without considering losses in the

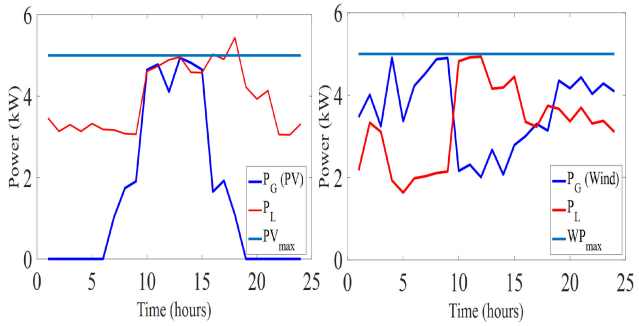

FIGURE 13. Profiles for daily generation and loads at microgrid-1 and 2 at 618^{th} iteration.

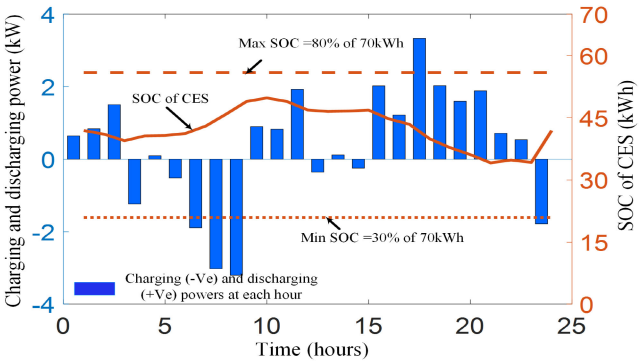

FIGURE 14. Daily charge and discharge cycles of CES.

TABLE 3. Simulation Parameters

Description	Parameter	Symbol	Value
UAPCC	Port-1 voltage	V_1	380 V ±10%
	Port-2 voltage	V_s	± 60 V
	Port-3 voltage (CES voltage)	V_{inb}	48 V ±10%
	DC link voltage	V_{lk}	60 V ±2%
	Filter capacitors	C_1, C_{lk}, C_s, C_b	500uF, 2000uF, 50uF, 100uF
	Filter inductors	L_s, L_b	100mH, 20mH
	Port-1 converter control parameters	K_{pv}, K_{iv}, K_{ii}	0.8, 0.15, 0.025
	Port-2 converter control parameters	K_{pp}, K_{ip}, K_{pk}, K_{ik}	0.022, 0.6, 0.1, 0.01
	Port-3 converter control parameters	K_{pb}, K_{ib}	0.1, 0.5
	Switching frequency	F_{sw}	10kHz
Distribution line	Line resistance	r_1 and r_2	2Ω
Microgrids	Bus voltages	V_1 and V_2	380 V ±5%

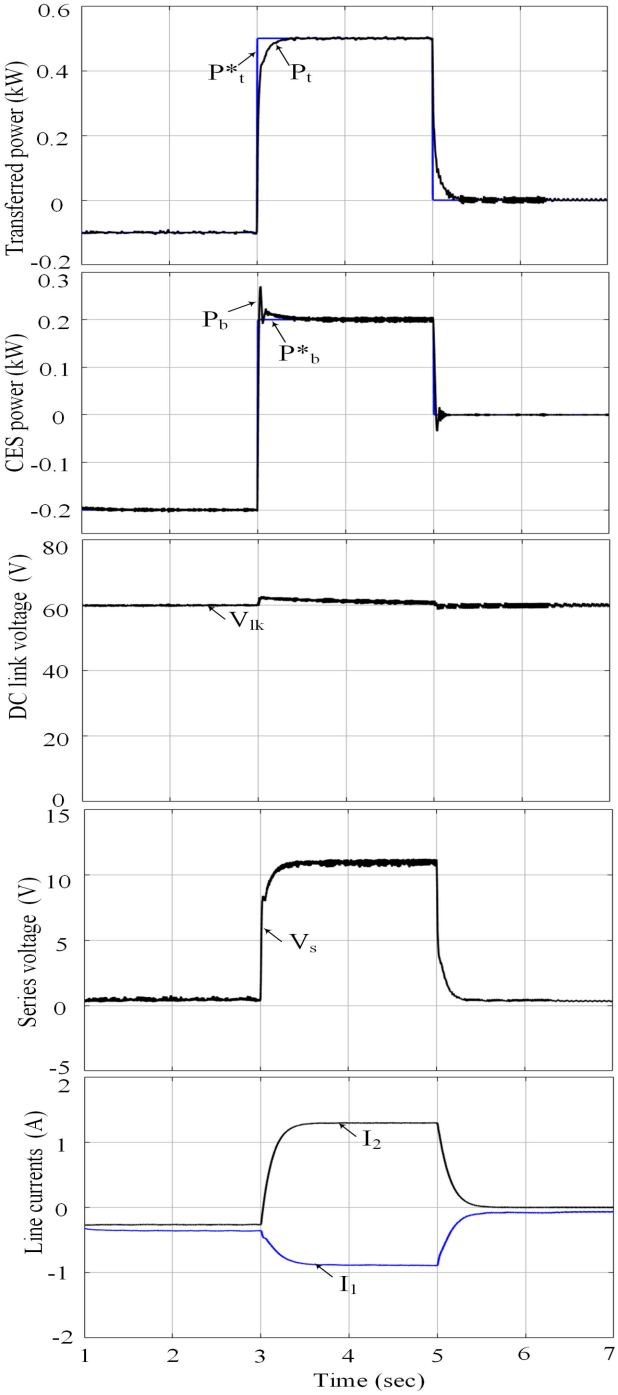

FIGURE 15. Dynamic response of the system.

converter is shown in Fig. 16. Therefore, the excess power will be transfered to CES which increases the utilization of renewable generation at both the grids.

B. POWER FLOW FROM CES AND GRID-1 TO GRID-2

This situation may occur when the load at grid-2 is increased suddenly or generation power is not sufficient to feed the load demand. The required power at grid-2 (500 W) is supplied by grid-1 (300 W) and CES (200 W) based on the command signal generated from RPSL (from 3 sec to 5 sec in a Fig. 15). The pictorial representation of power flow directions without considering losses in the converter is shown in Fig. 17. From this figure, it clearly indicates that power flowing in the line before UAPCC is 300 W and after UAPCC is 500 W. Therefore, with help of CES support, the overall losses ($I_1^2 r_1 + I_2^2 r_2$) in the system is reduced.

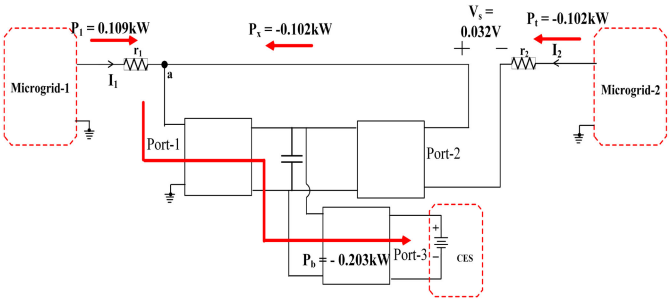

FIGURE 16. Pictorial representation of power flow from both the grids to CES.

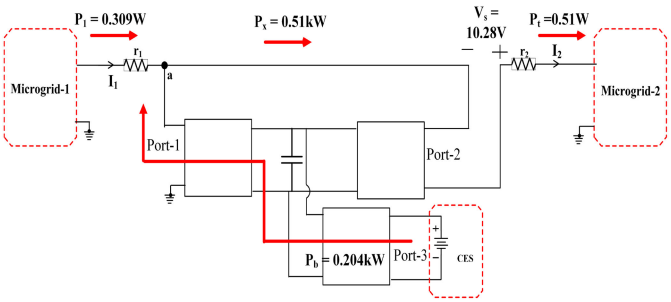

FIGURE 17. Pictorial representation of power flow from grid-1 and CES to grid-2.

C. NO POWER FLOW BETWEEN GRIDS AND CES

It is considered that both the microgrids are operating in normal condition (i.e., generation power is equal to load demand). Then there is no power flow requirement between grids and CES. In this situation, RPSL gives zero power commands (P_t^* and P_b^*) to port-2 and port-3 converters. The magnitude of I_2 indicates the power flow is zero towards the grid-2. But the magnitude of current I_1 is non-zero (in Fig. 15 from 5 sec to 7 sec) because a small amount of power is consumed by UAPCC to supply its operational uses.

D. EFFICIENCY ANALYSIS OF UAPCC

For the sake of analysis, two interconnected microgrids are considered, as shown in Fig. 3. It is assumed that the voltages at grid-1 and grid-2 are set at 380 V, with $r_1 = r_2 = 5\Omega$, and 500 W of power is transferred between grid-1 and grid-2. The CES support is considered to be 300 W (i.e., 60% of the power transferred). The complete system is simulated in PLECSIM and efficiency plots are shown in Fig. 18. The total losses in the system are plotted with different power flow conditions for two case studies (i.e. with and without CES), as shown in Fig. 19. From these results, it clearly indicates that the losses of the system in case-2 (i.e., with CES support) are less as compared to case-1 (i.e., without CES support). This proves that the line losses are reduced and the efficiency of the system is improved by considering CES for interconnected microgrid system. The asymmetric structure of the proposed converter (UAPCC) results in slightly different losses depending on the ports through which the power is processed. Here, two different power flow paths are shown in Fig. 20 considering discharging of CES. The losses are calculated up to a power transfer of 3 kW, as shown in Fig. 21. From this figure, it is observed that the difference (while considering two paths of power flow) is very small compared to power transferred in the line.

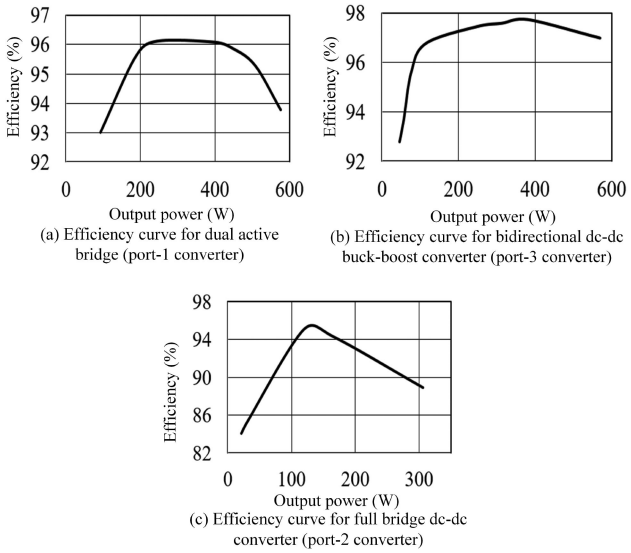

FIGURE 18. Efficiency plots of UAPCC converters.

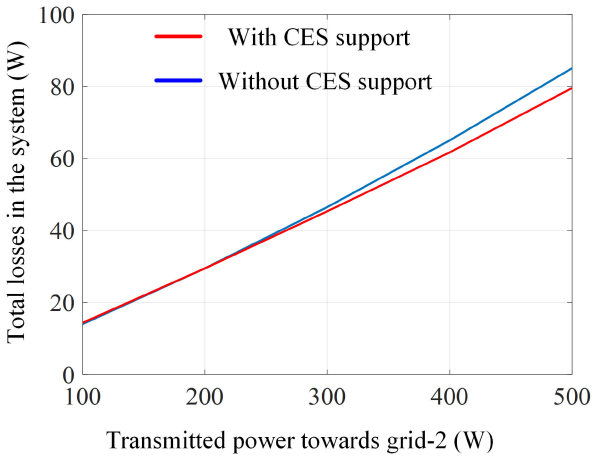

FIGURE 19. Transmitted Power vs. total system losses.

VII. EXPERIMENTAL RESULTS

An experimental setup of two interconnected dc microgrids and UAPCC is developed in the laboratory scale. The dc microgrid-1 is emulated with the help of programmable dc power supply (DC 380 V) with dc electronic load (187Ω) and dc microgrid-2 is emulated using 3-phase diode bridge rectifier with a resistive load (187Ω) as shown in Fig. 22 (a) and (b) respectively. The prototype of UAPCC with 48 V battery bank is shown in Fig. 22 (c). Two 5Ω (300 W) resistors are connected between microgrids which represent equivalent resistances of distribution line. Semikron make half-bridge IGBT module (SKM74GB12T4) is used to make the UAPCC.

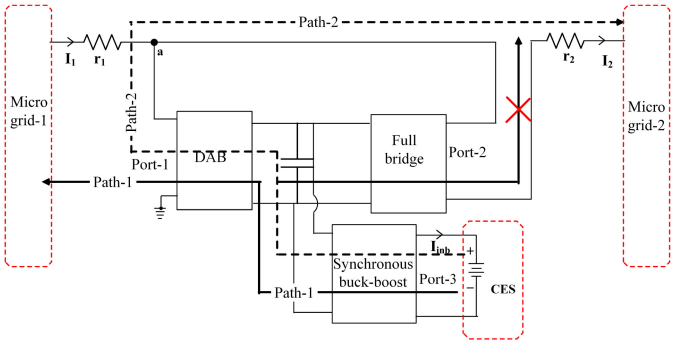

Path-1: power exchange is occurred between CES and microgrid-1
Path-2: power exchange is occurred between CES and microgrid-2

FIGURE 20. Pictorial representation of power exchange form CES to grids.

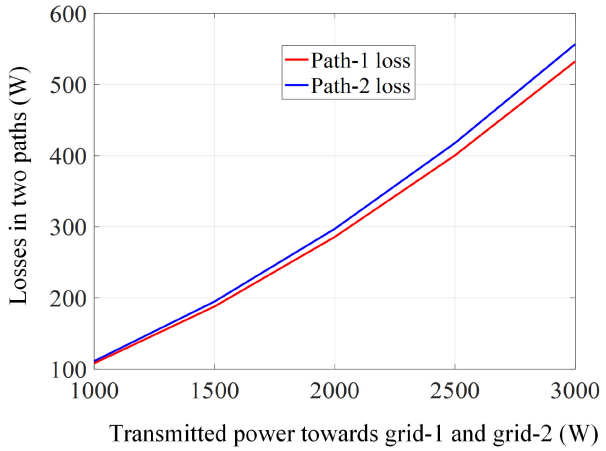

FIGURE 21. Loss in two paths for different power flow conditions.

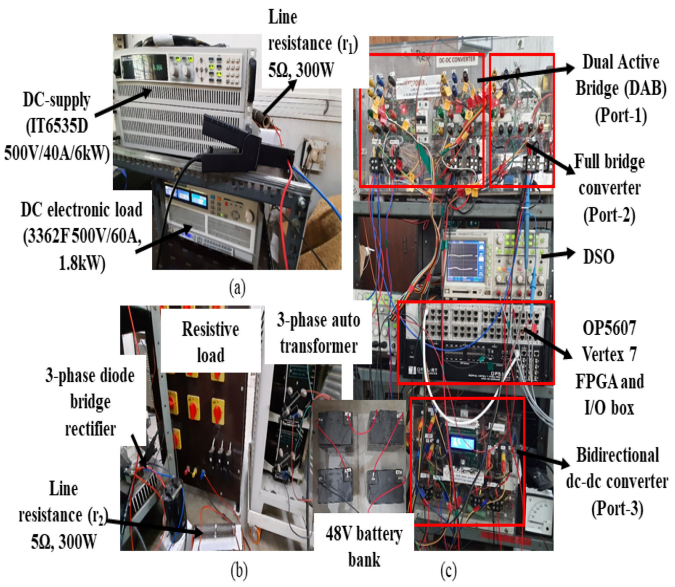

FIGURE 22. Experimental setup: (a) Emulation of dc microgrid-1, (b) Emulation of dc microgrid-2, and (c) UAPCC with battery bank.

TABLE 4. Parameters of Experimentation

Description	Parameter	Value
UAPCC	Port-1 voltage (V_1)	380 V ±10%
	Port-2 voltage (V_s)	± 60 V
	Port-3 voltage (V_{inb})	48 V ±10%
	DC link voltage (V_{lk})	60 V ±2%
	Filter capacitors (C_1, C_{lk}, C_s, C_b)	1000uF@450V, 2000uF@450V, 15uF@100V, 470uF@450V
	Filter inductors (L_s, L_b)	8mH, 1mH
	Switching frequency (F_{sw})	10kHz
	CES capacity	48 V, 28 AH
	Transformer turns ration	34 : 6
	Material and size of transformer and inductors	N-87 and E65
	Controller	OPAL-RT/OP5607
	IGBT modules	SKM74GB12T4
Distribution line	Line resistance (r_1 and r_2)	5Ω
Microgrids	Bus voltages (V_1 and V_2)	380 V ±5%

TABLE 5. Power Data for Experimental Results With Different Operating Modes

Different Power Flow (PF) control modes between grid-1(G-1), grid-2 (G-2) and CES	The net-power (kW)		Outputs from RPSL (kW)	
	at grid-1 (P_1)	at grid-2 (P_2)	P_t^*	P_b^*
M-1 (PF from G-1 and CES to G-2)	+0.3	-0.5	+0.5	+0.2
M-2 (PF from G-1 to CES and G-2)	+0.5	-0.3	+0.3	-0.2
M-3 (PF from G-2 and CES to G-1)	-0.5	+0.3	-0.3	+0.2
M-4 (PF from G-2 to CES and G-1)	-0.3	+0.5	-0.3	-0.2
M-5 (PF from CES to G-2)	0.0	-0.2	+0.2	+0.2
M-6 (PF from G-2 to CES)	0.0	+0.2	-0.2	-0.2
M-7 (PF from G-1 to CES)	+0.2	0.0	0.0	-0.2
M-8 (PF from CES to G-1)	-0.2	0.0	0.0	+0.2
M-9 (PF from CES to G-1 and G-2)	-0.1	-0.1	+0.1	+0.2
M-10 (PF from G-1 and G-2 to CES)	+0.1	+0.1	-0.1	-0.2
M-11 (PF from G-1 to G-2)	+0.5	-0.5	+0.5	0.0
M-12 (PF from G-2 to G-1)	-0.5	+0.5	-0.5	0.0
M-13 (No PF between G-1, G-2 and CES)	0.0	0.0	0.0	0.0

Remaining parameters of the hardware are mentioned in Table 4.

Table 5 indicates the power data for different operating modes. P_1 and P_2 are the net powers at grid-1 and 2 respectively (known values in this work). Here -ve sign indicates the power requirement i.e., P_G is less than P_L at the grids, whereas the excess power (P_G is more than P_L) is indicated by +ve sign; P_t^* is the reference power command to the port-2 converter, +ve sign indicates the power flow from grid-1 to grid-2 and -ve indicates opposite direction of power flow; P_b^* is the reference power command to the port-3 converter, +ve sign indicates the discharging operation and -ve sign is for charging.

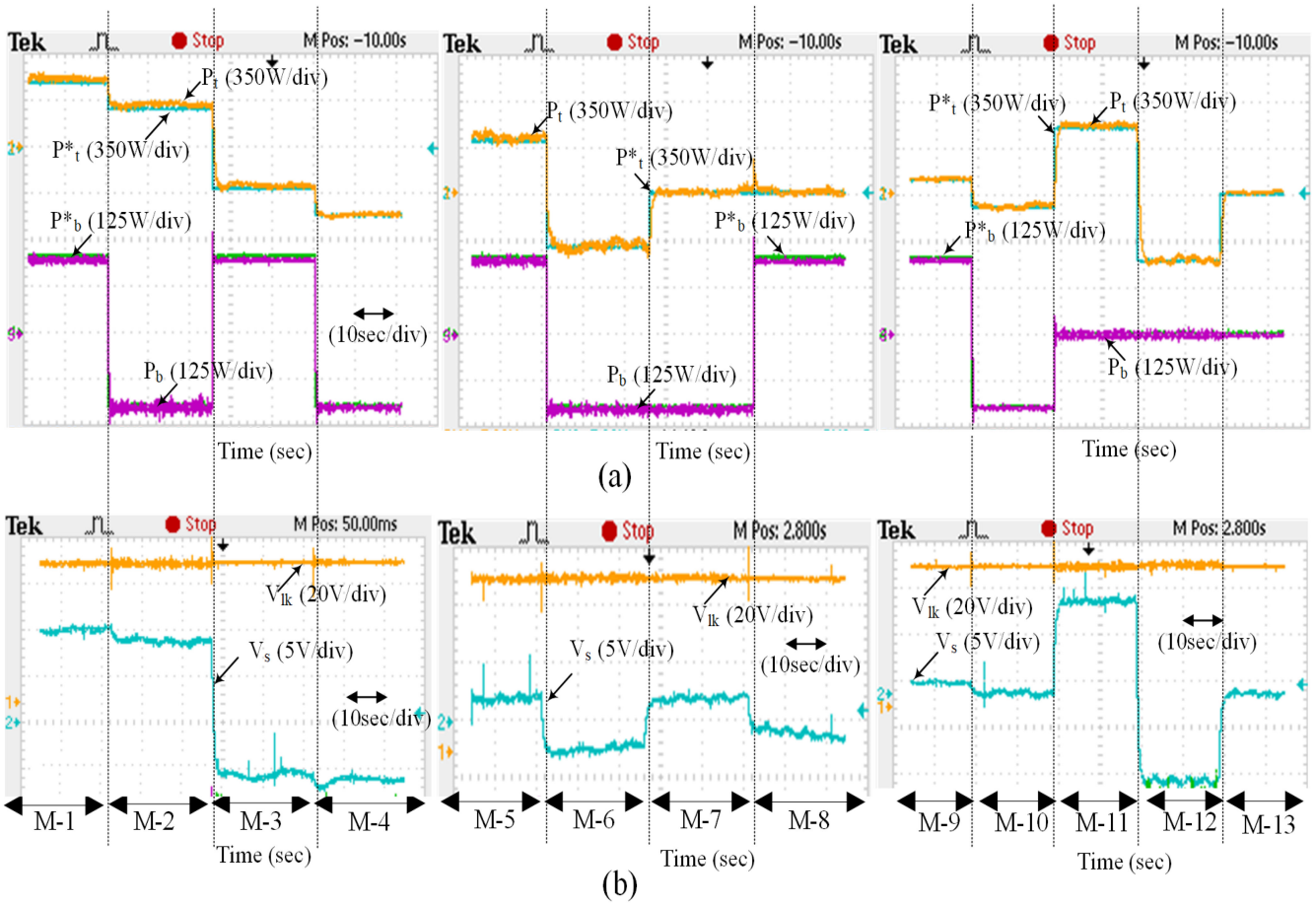

FIGURE 23. Dynamic response of the system: (a) transfered power (P_t) and CES power (P_b), (b) Output voltage of DAB (V_{lk}) and voltage injected in seres with the line (V_s).

Fig. 23 shows the dynamic response of Power Flow (PF) control in thirteen modes of operation corresponding in Table 5. In mode-1, it is considered that the net power ($P_2 = -500$ W) demand (including the discharging capacity of each local energy storage) is more than the excess power ($P_1 = +300$ W) at grid-1 (including the charging capacity of each local energy storage). To meet the load demand at grid-2, CES is supplying reaming 200 W which is indicated by P_b. and total transfered power ($P_t = +500$ W) in the distribution line towards the grid-2 are shown in Fig. 23 (a). The corresponding series injected voltage (V_s) and dc-link voltage (V_{lk}) are shown in Fig. 23 (b).

In mode-2, net power demand at grid-2 is suddenly reduced ($P_2 = -300$ W) and net excess power at grid-1 is increased ($P_1 = +500$ W). Now, CES is in charging operation, which increases the utilization of renewable generation. Fig. 23 (a) shows the polarity of battery power (i.e., $P_b = -200$ W), which is negative (charging). Note that the transfered power (P_t) is positive (towards grid-2) and the magnitude is reduced to 300 W. The corresponding series voltage (V_s) injected by the port-2 is also reduced.

In mode-3, opposite scenario of mode-2 takes place, where the generation at grid-2 is suddenly increased ($P_2 = +300$ W) and generation at grid-1 is reduced ($P_1 = -500$ W). In this case, the available excess net power (P_2) at grid-2 is not sufficient to meet the net required power (P_1) at grid-1. Therefore CES is supplying remaining 200 W (P_b), which reduces the load shut-down at grid-1. The direction of transfered power (P_t) is now changed to -ve (i.e., $P_t = -300$ W) to make the power flow away from grid-2. The corresponding series voltage (V_s) injected by port-2 is also changed its polarity.

Similarly, in all modes of operation, as shown in Fig. 23(a), P_t and P_b are tracking their reference power commands based on the RPSL. Corresponding series injected voltage (V_s) is changing its magnitude and polarity to transfer the required power. Fig. 23(b) shows the dc-link voltage (i.e., DAB output V_{lk}) which is always maintained constant (60 V) to its reference value in all modes of operation.

VIII. CONCLUSION

The universal active power control converter with common energy storage for interconnected microgrids is presented in this paper. The proposed configuration has the ability to control power transfer from one grid to another when grids have surplus/deficit of power. Inclusion of CES increases the utilization of renewable energy sources and reduces the lines

losses in the system by supporting additional active power. The proposed configuration is effective for RES dominated grids which always face uncertainty due to intermittency in generation. A method to estimate the size of the CES is also presented. Simulation and Experimental verification using OPAL-RT have confirmed the usefulness of the proposed system.

REFERENCES

[1] Q. Shafiee, Č. Stefanović, T. Dragičević, P. Popovski, J. C. Vasquez, and J. M. Guerrero, "Robust networked control scheme for distributed secondary control of islanded microgrids," *IEEE Trans. Ind. Electron.*, vol. 61, no. 10, pp. 5363–5374, Oct. 2014.

[2] S. Parhizi, H. Lotfi, A. Khodaei, and S. Bahramirad, "State of the art in research on microgrids: A review," *IEEE Access*, vol. 3, pp. 890–925, 2015.

[3] E. Hossain, R. Perez, A. Nasiri, and S. Padmanaban, "A comprehensive review on constant power loads compensation techniques," *IEEE Access*, vol. 6, pp. 33 285–33305, 2018.

[4] D. Kumar, F. Zare, and A. Ghosh, "DC microgrid technology: System architectures, ac grid interfaces, grounding schemes, power quality, communication networks, applications, and standardizations aspects," *IEEE Access*, vol. 5, pp. 12 230–12256, 2017.

[5] C. Li, F. de Bosio, F. Chen, S. K. Chaudhary, J. C. Vasquez, and J. M. Guerrero, "Economic dispatch for operating cost minimization under real-time pricing in droop-controlled dc microgrid," *IEEE J. Emerg. Sel. Top. Power Electron.*, vol. 5, no. 1, pp. 587–595, Mar. 2017.

[6] F. Guo, L. Wang, C. Wen, D. Zhang, and Q. Xu, "Distributed voltage restoration and current sharing control in islanded dc microgrid systems without continuous communication," *IEEE Trans. Ind. Electron.*, vol. 67, no. 4, pp. 3043–3053, Apr. 2020.

[7] G. Buticchi, S. Bozhko, M. Liserre, P. Wheeler, and K. Al-Haddad, "On-board microgrids for the more electric aircraft-technology review," *IEEE Trans. Ind. Electron.*, vol. 66, no. 7, pp. 5588–5599, Jul. 2019.

[8] P. Magne, B. Nahid-Mobarakeh, and S. Pierfederici, "Active stabilization of dc microgrids without remote sensors for more electric aircraft," *IEEE Trans. Ind. Appl.*, vol. 49, no. 5, pp. 2352–2360, Sep./Oct. 2013.

[9] S. Yousefizadeh, J. D. Bendtsen, N. Vafamand, M. H. Khooban, T. Dragičević, and F. Blaabjerg, "EKF-based predictive stabilization of shipboard dc microgrids with uncertain time-varying load," *IEEE J. Emerg. Sel. Top. Power Electron.*, vol. 7, no. 2, pp. 901–909, Jun. 2019.

[10] X. Chen *et al.*, "Consensus-based distributed control for photovoltaic-battery units in a dc microgrid," *IEEE Trans. Ind. Electron.*, vol. 66, no. 10, pp. 7778–7787, Oct. 2019.

[11] P. A. Madduri, J. Poon, J. Rosa, M. Podolsky, E. A. Brewer, and S. R. Sanders, "Scalable dc microgrids for rural electrification in emerging regions," *IEEE J. Emerg. Sel. Topics Power Electron.*, vol. 4, no. 4, pp. 1195–1205, Dec. 2016.

[12] M. Kumar, S. C. Srivastava, S. N. Singh, and M. Ramamoorty, "Development of a control strategy for interconnection of islanded direct current microgrids," *IET Renewable Power Gener.*, vol. 9, no. 3, pp. 284–296, Apr. 2015.

[13] N. W. A. Lidula and A. Rajapakse, "Microgrids research: A review of experimental microgrids and test systems," *Renewable and Sustain. Energy Rev.*, vol. 15, no. 1, pp. 186–202, 2011.

[14] S. Mudaliyar, B. Duggal, and S. Mishra, "Distributed tie-line power flow control of autonomous dc microgrid clusters," *IEEE Trans. Power Electron.*, vol. 35, no. 10, pp. 11250–11266, Oct. 2020.

[15] M. Lee, W. Choi, H. Kim, and B. Cho, "Operation schemes of interconnected dc microgrids through an isolated bi-directional dc–dc converter," in *Proc. IEEE Appl. Power Electron. Conf. Expo.*, 2015, pp. 2940–2945.

[16] N. N *et al.*, "Quantifying the benefits of a solar home system-based dc microgrid for rural electrification," *Energies*, vol. 12, no. 5 pp. 1–22, 2019.

[17] S. Moayedi and A. Davoudi, "Distributed tertiary control of dc microgrid clusters," *IEEE Trans. Power Electron.*, vol. 31, no. 2, pp. 1717–1733, Feb. 2016.

[18] X. Li *et al.*, "Flexible interlinking and coordinated power control of multiple dc microgrids clusters," *IEEE Trans. Sustain. Energy*, vol. 9, no. 2, pp. 904–915, Apr. 2018.

[19] K. Rouzbehi, J. I. Candela, A. Luna, G. B. Gharehpetian, and P. Rodriguez, "Flexible control of power flow in multiterminal dc grids using dc–dc converter," *IEEE J. Emerg. Sel. Topics Power Electron.*, vol. 4, no. 3, pp. 1135–1144, Sep. 2016.

[20] K. Natori, H. Obara, K. Yoshikawa, B. C. Hiu, and Y. Sato, "Flexible power flow control for next-generation multi-terminal dc power network," in *Proc. IEEE Energy Convers. Congr. Expo.*, 2014, pp. 778–784.

[21] T. L. Nguyen, J. M. Guerrero, and G. Griepentrog, "A self-sustained and flexible control strategy for islanded dc nanogrids without communication links," *IEEE J. Emerg. Sel. Top. Power Electron.*, vol. 8, no. 1, pp. 877–892, Mar. 2020.

[22] A. S. Morais and L. A. Lopes, "Interlink converters in dc nanogrids and its effect in power sharing using distributed control," in *Proc. IEEE 7th Int. Syp. Power Electron. Distrib. Gener. Syst.*, 2016, pp. 1–7.

[23] S. Balasubramaniam, C. E. Ugalde-Loo, and J. Liang, "Series current flow controllers for dc grids," *IEEE Access*, vol. 7, pp. 14 779–14790, 2019.

[24] A. Mohamed and O. Mohammed, "Smart power flow control in dc distribution systems involving sustainable energy sources," in *Proc. IEEE/PES Transmiss. Distrib. Conf. Exposition: Latin Amer.* (T&D-LA), 2010, pp. 372–379.

[25] K. Natori, T. Tanaka, Y. Takahashi, and Y. Sato, "A study on high-efficiency floating multi-terminal power flow controller for next-generation dc power networks," in *Proc. IEEE Energy Conversion Congr. Exposition*, 2017, pp. 2631–2637.

[26] U. Vuyyuru, S. Maiti, and C. Chakraborty, "Active power flow control between dc microgrids," *IEEE Trans. Smart Grid*, vol. 10, no. 5, pp. 5712–5723, Sep. 2019.

[27] D. An, Q. Yang, W. Yu, X. Yang, X. Fu, and W. Zhao, "Sto2Auc: A stochastic optimal bidding strategy for microgrids," *IEEE Internet Things J.*, vol. 4, no. 6, pp. 2260–2274, Dec. 2017.

[28] H. Zou, S. Mao, Y. Wang, F. Zhang, X. Chen, and L. Cheng, "A survey of energy management in interconnected multi-microgrids," *IEEE Access*, vol. 7, pp. 72 158–72169, May 2019.

[29] P. C. Loh, D. Li, Y. K. Chai, and F. Blaabjerg, "Autonomous control of interlinking converter with energy storage in hybrid ac–dc microgrid," *IEEE Trans. Ind. Appl.*, vol. 49, no. 3, pp. 1374–1382, May/Jun. 2013.

[30] D. Chen and L. Xu, "Autonomous dc voltage control of a dc microgrid with multiple slack terminals," *IEEE Trans. Power Syst.*, vol. 27, no. 4, pp. 1897–1905, Nov. 2012.

[31] E. Sortomme, M. M. Hindi, S. D. J. MacPherson, and S. S. Venkata, "Coordinated charging of plug-in hybrid electric vehicles to minimize distribution system losses," *IEEE Trans. Smart Grid*, vol. 2, no. 1, pp. 198–205, Mar. 2011.

[32] B. Zhao, Q. Song, W. Liu, and Y. Sun, "Overview of dual-active-bridge isolated bidirectional dc–dc converter for high-frequency-link power-conversion system," *IEEE Trans. Power Electron.*, vol. 29, no. 8, pp. 4091–4106, Aug. 2014.

[33] S. Shao, H. Chen, X. Wu, J. Zhang, and K. Sheng, "Circulating current and ZVS-on of a dual active bridge dc–dc converter: A review," *IEEE Access*, vol. 7, pp. 50 561–50572, Jan. 2019.

[34] M. Saeed, M. R. Rogina, A. Rodríguez, M. Arias, and F. Briz, "SiC-based high efficiency high isolation dual active bridge converter for a power electronic transformer,"*Energies*, vol. 13, no. 5, p. 1198, 2020.

[35] S. Inoue and H. Akagi, "A bidirectional dc–dc converter for an energy storage system with galvanic isolation," *IEEE Trans. Power Electron.*, vol. 22, no. 6, pp. 2299–2306, Nov. 2007.

[36] N. Mohan, T. M. Undeland, and W. P. Robbins, *Power Electronics: Converters, Applications, and Design*. Hoboken, NJ, USA: Wiley, 2003.

[37] R. W. Erickson and D. Maksimović, *Fundamentals of Power Electronics*. New York, NY, USA: Springer-Verlag, 2001.

[38] U. Vuyyuru, S. Maiti, C. Chakraborty, and B. C. Pal, "A series voltage regulator for the radial DC microgrid," *IEEE Trans. Sustain. Energy*, vol. 10, no. 1, pp. 127–136, Jan. 2018.

[39] D. Chen, L. Xu, and L. Yao, "DC voltage variation based autonomous control of dc microgrids," *IEEE Trans. Power Del.*, vol. 28, no. 2, pp. 637–648, Apr. 2013.

[40] A. Hussain, V.-H. Bui, and H.-M. Kim, "Robust optimization-based scheduling of multi-microgrids considering uncertainties," *Energies*, vol. 9, no. 4, p. 278, 2016.

[41] A. H. Hajimiragha, C. A. Canizares, M. W. Fowler, S. Moazeni, and A. Elkamel, "A robust optimization approach for planning the transition to plug-in hybrid electric vehicles," *IEEE Trans. Power Syst.*, vol. 26, no. 4, pp. 2264–2274, Nov. 2011.
[42] D. Bertsimas, E. Litvinov, X. A. Sun, J. Zhao, and T. Zheng, "Adaptive robust optimization for the security constrained unit commitment problem," *IEEE Trans. Power Syst.*, vol. 28, no. 1, pp. 52–63, Feb. 2013.
[43] Z. Wang, B. Chen, J. Wang, J. Kim, and M. M. Begovic, "Robust optimization based optimal DG placement in microgrids," *IEEE Trans. Smart Grid*, vol. 5, no. 5, pp. 2173–2182, Sep. 2014.
[44] S. X. Chen, H. B. Gooi, and M. Q. Wang, "Sizing of energy storage for microgrids," *IEEE Trans. Smart Grid*, vol. 3, no. 1, pp. 142–151, Mar. 2012.

UMAMAHESWARARAO VUYYURU (Student Member, IEEE) received the B.Tech. degree in electrical and electronics engineering from Jawaharlal Nehru Technological University, Kakinada, Kakinada, India and the M.Tech. degree in electrical engineering with specialization in power electronics from the National Institute of Technology Tiruchirappalli, Tiruchirappalli, India, in 2009 and 2012, respectively. He is currently working toward the Ph.D. degree with the School of Energy Science and Engineering, Indian Institute of Technology Kharagpur, Kharagpur, India. From 2012 to 2015, he was as an Assistant Professor with the GVP College of Engineering, Visakhapatnam, India. He was working on several research studies as a Research Collaborator with the Department of Electrical and Electronic Engineering, Imperial College London, London, U.K. His research interests include dc microgrids, power flow control, protection, and power electronic converters. He is a frequent Reviewer for the IEEE TRANSACTIONS ON SUSTAINABLE ENERGY, the IEEE TRANSACTIONS ON SMART GRIDS, the IEEE TRANSACTIONS ON INDUSTRIAL ELECTRONICS, the IEEE ACCESS, and the IEEE IES sponsored conferences.

SUMAN MAITI (Member, IEEE) received the B.E. degree in electrical engineering from Jalpaiguri Government Engineering College, Jalpaiguri, India, in 2002, the M.E. degree in electrical engineering from the Indian Institute of Engineering Science and Technology Shibpur, Howrah, India, in 2004, and the Ph.D. degree in electrical engineering from the Indian Institute of Technology Kharagpur, Kharagpur, India, in 2009. Since 2009, he has been with the Research and Development Group, ABB Ltd., Bengaluru, India, as an Associate Scientist. In 2014, he joined the Department of Electrical Engineering, Indian Institute of Technology Kharagpur as an Assistant Professor. His research interests include topology evaluation and control of multilevel converters for high power applications, ac/dc microgrids, and renewable energy integration and related issues.

CHANDAN CHAKRABORTY (Fellow, IEEE) received the B.E. and M.E. degrees in electrical engineering from Jadavpur University, Kolkata, India, in 1987 and 1989, respectively, and the Ph.D. degree in electrical engineering from the Indian Institute of Technology Kharagpur, Kharagpur, India, and Mie University, Tsu, Japan, in 1997 and 2000, respectively. He is currently a Professor with the Department of Electrical Engineering, and the Associate Dean of Sponsored Research and Industrial Consultancy, Indian Institute of Technology Kharagpur. His research interests include power converters, motor drives, electric vehicles, and renewable energy. During 2000—2002, he was the recipient of the JSPS Fellowship to work with the University of Tokyo, Tokyo, Japan and the IEEE Bimal Bose Energy Systems Award in 2019. He has regularly contributed to IES conferences such as IECON, ISIE, and ICIT as the Technical Program Chair/Track Chair. He was an Associate Editor for the IEEE TRANSACTIONS ON SUSTAINABLE ENERGY, the IEEE JOURNAL OF EMERGING AND SELECTED TOPICS IN INDUSTRIAL ELECTRONICS, the IEEE TRANSACTIONS ON INDUSTRIAL ELECTRONICS, and the *IEEE Industrial Electronics Magazine*. He is the Founding Editor-in-Chief of the IE Technology News, a web-only publication for the IEEE Industrial Electronics Society. From 2018 to 2019, he was the Co-Editor-in-Chief of the IEEE TRANSACTIONS ON INDUSTRIAL ELECTRONICS. He is currently the Editor-in-Chief for the IEEE JOURNAL OF EMERGING AND SELECTED TOPICS IN INDUSTRIAL ELECTRONICS. He is a Fellow of the Indian National Academy of Engineering.

EFSTRATIOS I. BATZELIS (Senior Member, IEEE) received the Ph.D. degree from the National Technical University of Athens, Athens, Greece, in 2016. He has been a Lecturer with the University of Southampton, Southampton, U.K., since April 2021 and a Research Fellow of the Royal Academy of Engineering working on solar integration in developing countries. His research interests include renewable energy technologies and distributed energy resources, mainly solar photovoltaics, power electronics control, and power system stability. He is currently an Associate Editor for the IEEE TRANSACTIONS ON SUSTAINABLE ENERGY. From 2017 to 2019, he was an EU Marie-Curie individual fellow of photovoltaic control and integration with Imperial College London, London, U.K., where since 2019, he has been a Research Fellow.